PHYSICAL REVIEW A **88**, 031401(R) (2013)

Production and trapping of cold circular Rydberg atoms

D. A. Anderson,* A. Schwarzkopf, R. E. Sapiro, and G. Raithel
Department of Physics, University of Michigan, Ann Arbor, Michigan 48109, USA
(Received 21 May 2013; published 16 September 2013)

Cold circular Rydberg atoms are produced and magnetically trapped. The trap is characterized by direct spatial imaging of ion distributions, ion counting, and state-selective field ionization. At room temperature, we observe about 70% of the trapped atoms remaining after 6 ms. We measure a trap oscillation frequency increase of the circular Rydberg atom trap relative to the ground-state atom trap due to the larger magnetic moment of the circular Rydberg atoms. Simulations of the center-of-mass and internal-state evolution of circular states in our magnetic trap are performed and results are in good agreement with experimental observations.

DOI: 10.1103/PhysRevA.88.031401 PACS number(s): 32.10.Ee, 32.10.Dk, 37.10.Jk

Circular Rydberg states [1] correspond to highly excited, Bohr-like electron trajectories with maximal orbital angular momenta. Circular-state (CS) atoms exhibit a unique combination of extraordinary properties: long lifetimes, large magnetic moments, and no first-order Stark shift. These features have made CS atoms attractive for cavity quantum electrodynamics experiments [2,3], where the CS atoms provide a near-perfect two-level system for probing atom-cavity interactions. Precision measurements [4,5] benefit from the reduced nuclear and QED perturbations of these high-angular-momentum states. The large angular momenta also make CS atoms intriguing candidates for studies of interactions between Rydberg and ground-state atoms, such as the generation of Rydberg-ground molecules with GHz binding energies [6,7].

Several applications would benefit from trapping CS Rydberg atoms. While optical, electrostatic, and high-gradient magnetic trapping methods have been considered [8–10] and demonstrated [11–14] for atoms in other Rydberg states, cold, pure CS atoms have, to our knowledge, neither been prepared nor trapped. Additionally, magnetic Rydberg trapping has previously only been achieved for mixtures of Rydberg states, not for well-defined quantum states. In this Rapid Communication we describe the generation and trapping of cold, pure CS atoms in a conventional magnetic trap. We produce CS atoms at temperatures several orders of magnitude lower than in previous experiments (see, for example, [1,3,15,16]) and magnetically trap them. We employ the trapping force to measure their magnetic moments, which are the largest used in atom trapping to date. We characterize the trap using ion detection schemes that provide information on the center-of-mass (COM) oscillations in the trap, trap losses, and the atomic internal-state evolution.

We begin with a sample of $\sim 10^7$ ^{87}Rb atoms magnetically trapped in the $|F = 2, m_F = 2\rangle$ ground state at a temperature ~ 100 μK and density $\sim 10^{10}$ cm^{-3}. The Ioffe-Pritchard-type magnetic trap is generated using a Z-shaped wire [17]. The cigar-shaped trap has trap frequencies $(\omega_{x'},\omega_{y'},\omega_{z'}) = 2\pi \times (7.9 \pm 0.3, 39.6 \pm 0.1, 37.4)$ Hz, where $\omega_{x'}$ and $\omega_{y'}$ are measured and $\omega_{z'}$ is calculated. The trap field minimum is measured to be 5.7 ± 0.6 G and is located 3.5 ± 0.2 mm from the surface of the Z wire. A schematic of the experiment and a plot of the magnetic field strength are shown in Fig. 1. The magnetic trapping region is enclosed by an electrode structure consisting of six individually addressable electrodes. Electric fields are controlled with an accuracy of $\leqslant 30$ mV/cm in all coordinates using voltage-to-field calibration factors and field zeros obtained from Stark spectroscopy [18] on $85D$ Rydberg states. Electrode "T" is used for Rydberg-atom field ionization and electrode "B" produces an electric-field ramp required for the CS production. A microchannel plate (MCP) is located 10 cm from the excitation region, outside of the electrode package, and is used for ion detection (30% efficiency) and imaging.

We generate CS atoms with principal quantum number $n = 57$ by the crossed-fields method [19]. We first optically excite, in the presence of an electric field $\mathbf{E} = -E\hat{\mathbf{z}}$ from the B electrode (see Fig. 1), into the highest-lying state of the manifold of $n = 57$ states that exhibit the linear Stark effect ("hydrogenic states"). The excitation is done with counterpropagating 480 and 780 nm laser beams. The fixed-frequency 780 nm laser is 1 GHz off-resonance from the $5S_{1/2}$ to $5P_{3/2}$ transition; the 480 nm laser is tunable to excite Rydberg levels. The combined excitation bandwidth is $\nu_L \approx 2$ MHz. The 480 nm beam is focused to a waist of $w_0 = 50$ μm and the 780 nm beam is collimated to $w_0 = 1.5$ mm, with powers of 35 and 2 mW, respectively. Both beams are linearly polarized perpendicular to the axis of the applied electric field. At a field of ≈ 1.8 V/cm the $60P$ states intersect with the $n = 57$ hydrogenic states. This field also mixes enough S and D character into the P Rydberg states to enable two-photon excitation from the $5S_{1/2}$ ground state. Experimental and calculated two-photon excitation spectra are shown in Fig. 2. In the experimental spectrum the hydrogenic states appear only in regions where they intersect with $60P$ states. Due to the coupling between the states, the intersections are anticrossings with splittings of 20 MHz or more, as seen in Fig. 2(b). For our initial step in the CS production we excite to regions labeled I and II in Fig. 2(a).

After a 15 μs excitation pulse to region I, the electric field is ramped down over 40 μs from its initial value of 1.76 V/cm to 0 V/cm, within the residual electric-field uncertainty. This is slow enough to ensure adiabatic evolution of the Rydberg atoms within the anticrossings in Fig. 2. Regions labeled IV are not chosen because of state crossings at lower electric-field values that would cause state mixing during the electric-field ramp. The 5.7 G magnetic field at the bottom of the atom trap is always on and is perpendicular to the

*anderda@umich.edu

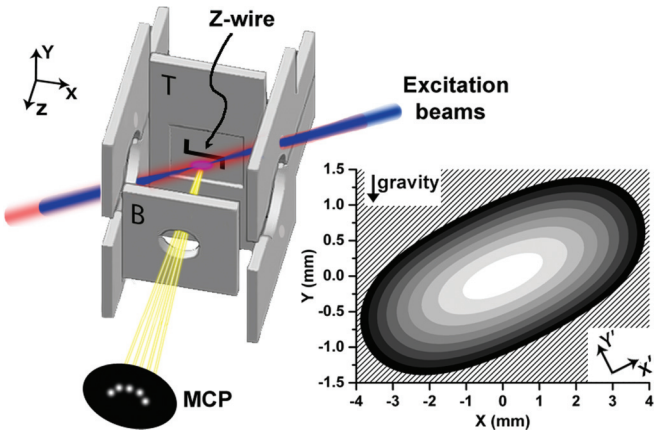

FIG. 1. (Color online) Left: schematic of the experiment (to scale). Six gold-coated, copper electrodes enclose a magnetically trapped atom sample to control the electric fields at the excitation location. An MCP is used for ion detection. The location of the Z wire and the counterpropagating 480 and 780 nm beams for excitation to Rydberg states are also shown. Right: plot of the magnetic field strength in the xy plane through the center of the trap. The linear gray scale ranges from $|B| = 5.5$ G (white) to 9.5 G (black) in steps of 0.5 G. The hatched region indicates $|B| \geqslant 10$ G.

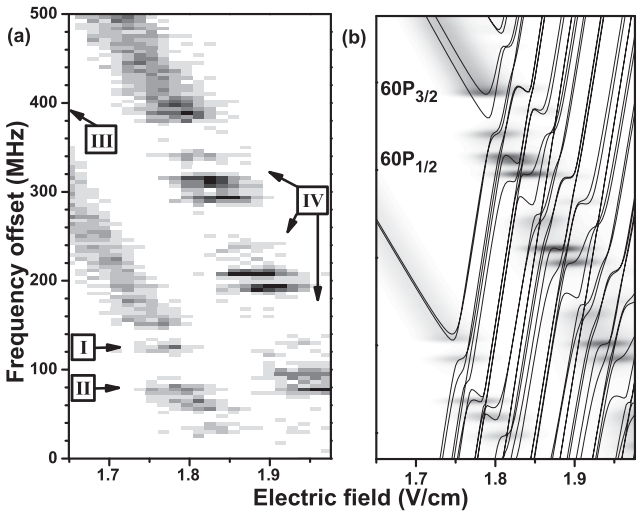

FIG. 2. (a) Experimental Stark spectrum showing the intersection of $60P$ with the $n = 57$ hydrogenic manifold. Plotted are average counts per excitation pulse [linear scale ranging from 0 (white) to >3.5 (black)] as a function of applied electric field and frequency offset of the 480 nm laser from an arbitrary reference frequency. Each data point is an average of 50 excitation pulses. The electric-field axis is scaled by a factor of 0.98 to match the calculation in (b). (b) Energy levels (solid lines) and excitation rates per atom calculated for our laser polarizations and intensities (overlay; linear gray scale from 0 to 150 s^{-1}). In the excitation-rate calculation we assume Gaussian distributions for the excitation frequency and electric field, with FWHM of 5 MHz and 50 mV/cm, respectively. Minor deviations in frequency between (a) and (b) are attributed to long-term excitation-laser drifts.

ramped electric field. At the end of the ramp, the Larmor frequency ($\omega_L = 2\pi \times 8$ MHz) is larger than the residual Stark frequency ($\omega_S = \frac{3nEea_0}{2\hbar} \lesssim 2\pi \times 3$ MHz, where e and a_0 are the electron charge and Bohr radius, respectively). In the adiabatic sweep from the Stark-dominated ($\omega_S > \omega_L$) to the Zeeman-dominated regime ($\omega_S < \omega_L$) the atoms initially prepared into region I in Fig. 2(a) evolve with near-unity probability into the $|n = 57,\ \ell = 56,\ m_\ell = 56,\ m_s = +0.5\rangle$ CS. The CS has good quantum numbers m_ℓ and m_s because in high-ℓ states the Zeeman effect dominates the fine structure. The magnetic field stabilizes the CS by lifting its degeneracy with any other hydrogenic state. The angular momentum of the trapped CS atom is parallel to the magnetic field at the trap minimum, which points along $\mathbf{x}'$ in Fig. 1. This CS is low-field seeking; the complementary $|n = 57,\ \ell = 56,\ m_\ell = -56,\ m_s = -0.5\rangle$ CS is unsuitable for magnetic atom trapping because it is high-field seeking.

Due to their large magnetic moments, CS atoms in a magnetic trap experience significantly deeper confining potentials than ground-state atoms. The magnetically trapped $|F = 2,\ m_F = 2\rangle$ atoms (Landé factor $g_F = \frac{1}{2}$) have a magnetic moment of one Bohr magneton, $\mu_{GS} = -\mu_B$. The CS atoms described above have a magnetic moment $\mu_{CS} = -\mu_B(m_\ell + g_s m_s) = -57\mu_B$, where $g_s \approx 2$. In a harmonic magnetic trap, the CS atom experiences a potential increase, $U_{CS} = (\frac{\mu_{CS}}{\mu_{GS}})U_{GS} = 57U_{GS}$, and a corresponding trap frequency increase, $\omega_{CS} = \sqrt{57}\omega_{GS}$, where U_{CS} and U_{GS} are the CS and ground-state magnetic potentials, and ω_{CS} and ω_{GS} are the CS and ground-state trap frequencies, respectively.

The minimum of the ground-state trap is substantially shifted due to gravity, while in the much stronger CS trap gravity can be ignored. The displacement vector pointing from the minimum of the ground-state trap to the minimum of the CS trap is calculated to be $\delta\mathbf{r} = (\delta x, \delta y, \delta z) = (710, 290, 0)\ \mu$m (using calculated force constants and the 12 ± 0.2 degree tilt of the trap with respect to gravity; see Fig. 1). This displacement allows us to initiate sloshing-mode oscillations of trapped CS atoms in the $\mathbf{x}'$ and $\mathbf{y}'$ directions.

To observe these oscillations we first generate the $|\mathrm{CS} - 1\rangle \equiv |n = 57,\ \ell = 56,\ m_\ell = 55,\ m_s = +0.5\rangle$ near CS by initial excitation to region II in Fig. 2. We excite to II because it provides a stronger experimental signal than I; both regions result in high-ℓ states that exhibit quantitatively similar trapping behavior. The expected trap period for the near CS is $T_{CS-1} = \frac{T_{GS}}{\sqrt{n-1}}$, which equals 16.9 and 3.4 ms in $\mathbf{x}'$ and $\mathbf{y}'$, respectively. Since the excitation and circularization time interval of 55 μs is much smaller than T_{CS-1}, the atoms are prepared on the side of their trapping potential U_{CS-1}, at the location $-\delta\mathbf{r}$. A field-ionization pulse is applied at varying time delays t_d from the end of the $|\mathrm{CS} - 1\rangle$ production. The ion positions are projected onto the MCP, where they generate spatially resolved light pulses on a phosphor screen, which is imaged by a CCD camera. The COM coordinates of the ion distributions in the MCP plane are obtained from sums of 2000 images at each t_d [20]. Plots of the $\mathbf{x}$ and $\mathbf{y}$ COM coordinates as a function of t_d are shown in Fig. 3. The $\mathbf{y}$ COM data [Fig. 3(a)] is fit to a sinusoid out to 4 ms from which we obtain an oscillation period of 3.4 ± 0.1 ms. This is in excellent agreement with the predicted value. The $\mathbf{y}$ COM data is only considered out to 4 ms because of distortions in the ion trajectories thereafter, as suggested by the $\mathbf{x}$ COM data. Since $\delta x \approx 2.5\delta y$, we expect a larger COM oscillation

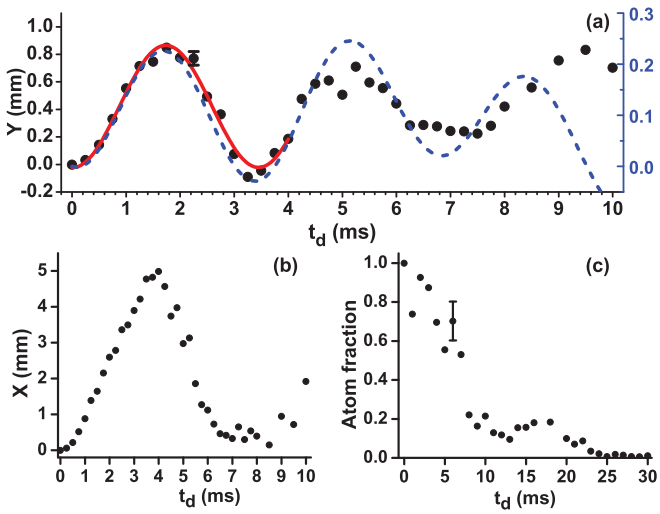

FIG. 3. (Color online) (a) Experimental COM displacement in **y** vs t_d (circles) in the MCP plane (left axis) with a fit to a sinusoid out to 4 ms (solid curve). The RMS spread of the data about the fit is 0.05 mm, indicated by the representative error bar. The simulated COM displacement in **y** vs t_d in the object plane (right axis) is shown out to 10 ms (dashed curve). A linear offset is subtracted to match the experimental data, accounting for ion-imaging abberations. (b) Experimental COM displacement in **x** vs t_d. (c) Fraction of detected atoms remaining vs t_d. Based on the variance of the data points, we estimate an uncertainty shown by the representative error bar.

amplitude in **x**. The **x** COM coordinate plotted in Fig. 3(b) develops a large displacement over about 4 ms. At $t_d = 4$ ms there is an apparent reversal in the direction of motion of the **x** COM coordinate, which occurs about a factor of 2 earlier than expected. We believe that the **x** COM oscillation amplitude is so large that it brings the ions produced by field ionization far enough off of the ion-imaging axis to cause distortion and obstruction [see Fig. 3(c) and discussion]. This prevents a direct measurement of the **x** COM oscillation period, as well as the **y** COM oscillation period after 4 ms.

To model the system, we perform Monte Carlo simulations of the internal-state evolution of a sample initially in the state $|\mathrm{CS}-1\rangle$ in a $T = 300$ K radiation background; atom trajectories inside the magnetic trapping field are computed classically. The internal-state evolution and trajectories are coupled. The simulations account for all radiative transitions, including thermal photoionization, but no collisions. Typically, the rate of thermally induced transitions per atom is 6×10^3 s^{-1}. (For comparison, in a $T = 4$ K cryogenic enclosure it would be 0.1×10^3 s^{-1}.) The rapid state evolution from the $|\mathrm{CS}-1\rangle$ due to the 300 K thermal radiation results in n, ℓ, and m redistribution of the initially prepared sample, leading to a time dependence of the average magnetic dipole force as well as a diffusive component of that force. The change in average m amounts to less than 1% over the 10 ms observation time. The corresponding change in average oscillation frequency is too small to be seen in the experiment. The diffusive component of the m evolution is more significant, reaching an rms spread of $\pm 15\%$ about the average m over 10 ms. This is large enough that we would expect some damping effect on the COM oscillations. From the simulations we obtain COM oscillation periods and decay constants of 16.5 and 36.2 ms in $\mathbf{x}'$ and 3.4 and 10.2 ms in $\mathbf{y}'$, respectively. In Fig. 3(a) we plot the simulated **y** COM oscillation with a linear offset subtracted to match the experiment, accounting for ion-imaging abberations. We test the importance of thermally driven m-state diffusion by turning off all radiative transitions in the simulation, leaving anharmonicity-induced dephasing as the sole source of damping. We find that m diffusion and trap anharmonicity contribute in approximately equal parts to the decay of the COM oscillations over 10 ms.

To measure the magnetic trapping time we plot the number of detected Rydberg atoms as a function of t_d. Figure 3(c) shows the fraction of Rydberg atoms detected relative to $t_d = 0$. We observe as much as 70% of the initially prepared sample remaining in the trap after 6 ms. If any $60P$ atoms remained after the circularization sequence, our simulations show that only a $\sim 5 \times 10^{-5}$ fraction of them would survive after 6 ms. From this we conclude that our circularization procedure is very efficient. Between 7 and 13 ms we measure a rapid drop in signal, as well as a significant resurgence at about 16 ms. We believe that the rapid drop is due to atoms moving out of the ion-imaging field of view (in the **x** direction), while the resurgence occurs because of atoms moving back into view. This scenario is consistent with both the expected **x** oscillation period (16.5 ms) as well as the early reversal of the **x** COM in Fig. 3(b).

From Fig. 3(c) we estimate an overall loss rate of $\gtrsim 50$ s^{-1} for the trapped CS population. This loss rate cannot be explained at a quantitative level, as low-velocity CS atoms were not available until now and data on their collision cross sections are not available. However, the loss rate is consistent with collisions between Rydberg and ground-state atoms being the primary loss mechanism. This is determined from collisional cross sections between Rb low-ℓ Rydberg and ground-state atoms provided in [21] and the estimated background Rb pressure. Losses from Rydberg-Rydberg collisions are not expected at the low Rydberg atom densities used (initially a few 10^6 cm^{-3}). Our simulations of the state evolution show a loss rate of about 0.5 s^{-1} (at 300 K and accounting for all noncollisional loss channels), which is negligible in comparison to the measured loss rate.

Given the influence of the internal-state dynamics on the trapping behavior, we probe the internal-state evolution by performing state-selective field ionization (SSFI) on the trapped Rydberg atom sample. A near-linear SSFI ramp is applied reaching a field of >120 V/cm over the course of 50 μs. Different Rydberg states ionize at different points on the ramp, and can be distinguished by arrival time at the detector. Figure 4(a) shows SSFI traces for excitation to region III in Fig. 2, where only $60P_{1/2}$ atoms are excited. In this case, the electric-field ramp in the circularization procedure fails to populate any atoms in the CS; all atoms remain in $60P_{1/2}$. Figure 4(b) shows SSFI traces for excitation to region I in Fig. 2, where the CS generation procedure is expected to circularize most of the atoms. In both cases we obtain SSFI traces for $t_d = 0$ and 1 ms. We first compare the integrals of the SSFI curves. Excitation to region I produces a long-lived signal (0.59 remaining fraction), while excitation to III does not (0.09 remaining fraction), reaffirming the high yield of long-lived CS atoms.

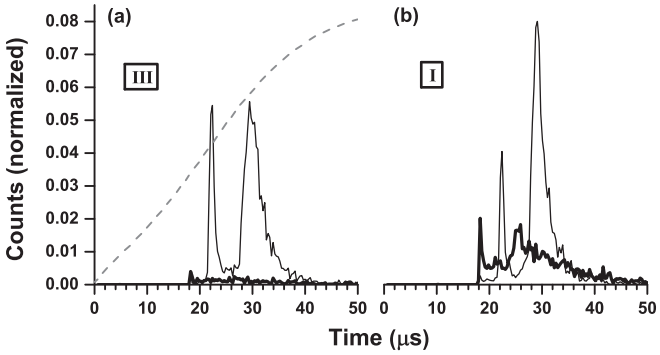

FIG. 4. SSFI traces for an initial excitation into two different regions in Fig. 2: (a) into III, the $60P_{1/2}$ state and (b) into I, the first anticrossing at the $60P$-manifold intersection to generate the CS after the circularization procedure. In both (a) and (b) the thin and thick traces correspond to $t_d = 0$ and 1 ms, respectively. Each trace is a sum of 20 000 experiments. The data are normalized such that for $t_d = 0$ ms the curves integrate to the same value. The dashed curve in (a) shows the field-ionization ramp used in both experiments.

Next we compare the structures of the SSFI curves. In both Figs. 4(a) and 4(b), with $t_d = 0$, there are two distinct peaks: an early (22 μs) peak, which we attribute to adiabatic field-ionization events, and a later (29 μs) diabatic, high-field-ionizing peak [22]. In Fig. 4(b), the diabatic peak for $t_d = 1$ ms arrives earlier than for $t_d = 0$ ms, and is substantially broadened. This indicates a reduced average ionization field for the trapped sample at later times (corresponding to a higher average n) and rapid state diffusion, respectively. An additional peak emerges at an even earlier arrival time (18 μs). This peak is attributed to atoms accumulating in extremely high-n Rydberg states. The trends in Fig. 4 are in qualitative agreement with our simulations, which also show a thermally driven redistribution of population to longer-lived, very high-n states. For experimental reasons the field ionization is performed in crossed electric and magnetic fields; a detailed modeling of the SSFI curves in Fig. 4 is beyond the scope of this paper.

In summary, we have demonstrated a room-temperature magnetic trap for cold CS Rydberg atoms with $n = 57$. The trap oscillation period and trapping time have been measured and are in good agreement with predicted values and detailed simulations. The internal-state evolution of the atom sample was probed, showing the effect of the 300 K blackbody radiation background on the n distribution in the trap. Our trapping method could be employed in a 4 K cryogenic environment to suppress thermal transitions and provide a source of long-lived CS atoms for precision measurements [4,5]. Our work on cold, trapped CS Rydberg atoms paves the way for studies of exotic quantum states. For example, at sufficiently high ground-state atom density high-ℓ Rydberg-ground molecules [6] may be produced in the generation of the CS. Due to their increased mass, these molecules would manifest as trailing signals in the COM oscillations of the CS in the magnetic trap. Another intriguing quantum object, which one could prepare in a setup similar to ours, would consist of a hollow electron wave function (that of the CS Rydberg atom) surrounding the ionic Rydberg-atom core and a Bose-Einstein condensate. This system would present an ideal platform to study interactions between ions and condensates [23–25].

This work was supported by the AFOSR (Grant No. FA9550-10-1-0453).

[1] R. G. Hulet and D. Kleppner, Phys. Rev. Lett. **51**, 1430 (1983).
[2] R. G. Hulet, E. S. Hilfer, and D. Kleppner, Phys. Rev. Lett. **55**, 2137 (1985).
[3] M. Brune, E. Hagley, J. Dreyer, X. Mâitre, A. Maali, C. Wunderlich, J. M. Raimond, and S. Haroche, Phys. Rev. Lett. **77**, 4887 (1996).
[4] J. Hare, A. Nussenzweig, C. Gabbanini, M. Weidemuller, P. Goy, M. Gross, and S. Haroche, IEEE Trans. Instrum. Meas. **42**, 331 (1993).
[5] R. Lutwak, J. Holley, P. P. Chang, S. Paine, D. Kleppner, and T. Ducas, Phys. Rev. A **56**, 1443 (1997).
[6] C. H. Greene, A. S. Dickinson, and H. R. Sadeghpour, Phys. Rev. Lett. **85**, 2458 (2000).
[7] V. Bendkowsky, B. Butscher, J. Nipper, J. P. Shaffer, R. Löw, and T. Pfau, Nature (London) **458**, 1005 (2009).
[8] S. K. Dutta, J. R. Guest, D. Feldbaum, A. Walz-Flannigan, and G. Raithel, Phys. Rev. Lett. **85**, 5551 (2000).
[9] W. H. Wing, Phys. Rev. Lett. **45**, 631 (1980).
[10] B. Hezel, I. Lesanovsky, and P. Schmelcher, Phys. Rev. Lett. **97**, 223001 (2006).
[11] S. E. Anderson, K. C. Younge, and G. Raithel, Phys. Rev. Lett. **107**, 263001 (2011).
[12] S. Zhang, F. Robicheaux, and M. Saffman, Phys. Rev. A **84**, 043408 (2011).
[13] S. D. Hogan and F. Merkt, Phys. Rev. Lett. **100**, 043001 (2008).
[14] J.-H. Choi, J. R. Guest, A. P. Povilus, E. Hansis, and G. Raithel, Phys. Rev. Lett. **95**, 243001 (2005).
[15] J. Hare, M. Gross, and P. Goy, Phys. Rev. Lett. **61**, 1938 (1988).
[16] R. Brecha, G. Raithel, C. Wagner, and H. Walther, Opt. Commun. **102**, 257 (1993).
[17] J. Reichel, W. Hänsel, and T. W. Hänsch, Phys. Rev. Lett. **83**, 3398 (1999).
[18] J. Neukammer, H. Rinneberg, K. Vietzke, A. König, H. Hieronymus, M. Kohl, H. J. Grabka, and G. Wunner, Phys. Rev. Lett. **59**, 2947 (1987).
[19] D. Delande and J. C. Gay, Europhys. Lett. **5**, 303 (1988).
[20] See Supplemental Material at http://link.aps.org/supplemental/10.1103/PhysRevA.88.031401 for a video sequence of composite images with increasing t_d.
[21] T. F. Gallagher, *Rydberg Atoms* (Cambridge University Press, New York, 1994), pp. 220–221.
[22] R. Stebbings and F. Dunning, *Rydberg States of Atoms and Molecules* (Cambridge University Press, New York, 1983), pp. 100–101.
[23] R. Côté, V. Kharchenko, and M. D. Lukin, Phys. Rev. Lett. **89**, 093001 (2002).
[24] R. Côté, Phys. Rev. Lett. **85**, 5316 (2000).
[25] R. Côté and A. Dalgarno, Phys. Rev. A **62**, 012709 (2000).